

<b>6</b>	<b>PERFORMANCE OF THE NOvA DESIGN</b>	<b>6-2</b>
6.1	A VISUAL OVERVIEW OF THE NOvA DETECTOR PERFORMANCE	6-2
6.2	NOvA PERFORMANCE LINKED TO CELL LIGHT OUTPUT AND THRESHOLD CUT	6-5
6.2.1	<i>Technical Requirement on the Threshold Cut</i>	6-5
6.2.2	<i>Required Light Level</i>	6-6
6.3	MEASURED PERFORMANCE OF MULTIPLE CELLS	6-7
6.4	NOvA SCIENTIFIC PERFORMANCE REQUIREMENT TRANSLATED INTO DESIGN CRITERIA	6-9
6.4.1	<i>Technical Design Criterion for the NOvA scintillator</i>	6-9
6.4.2	<i>Technical Design Criterion for the NOvA Wavelength Shifting Fiber</i>	6-9
6.4.3	<i>Technical Design Criterion for the NOvA PVC Extrusions</i>	6-10
6.4.4	<i>Technical Design Criterion for the NOvA Extrusion Modules</i>	6-10
6.4.5	<i>Technical Design Criterion for the NOvA Avalanche Photodiodes and Electronics</i>	6-10
6.4.6	<i>Aging Effects</i>	6-10
6.4.7	<i>Summary of Technical Design Criteria</i>	6-10
6.5	QUANTITATIVE PERFORMANCE ANALYSIS OF THE NOvA FAR DETECTOR	6-11
6.5.1	<i>Simulation and Reconstruction Package</i>	6-11
6.5.2	<i>Figure of Merit</i>	6-13
6.5.3	<i>Detector Energy Resolution for Neutrino Events</i>	6-16
6.6	SIMULATED PERFORMANCE OF THE NOvA NEAR DETECTOR	6-17
6.6.1	<i>Location and Orientation</i>	6-17
6.6.2	<i>Comparison of Event Spectra between Near and Far Detectors</i>	6-17
6.6.3	<i>Near Detector Timing Requirements</i>	6-19
6.7	SUMMARY: NOvA DESIGN PERFORMANCE VS. SCIENTIFIC DESIGN CRITERIA	6-21
6.8	CHAPTER 6 REFERENCES	6-22

# 6 Performance of the NOvA Design

## 6.1 A Visual Overview of the NOvA Detector Performance

About one-third of the neutrino interactions at NOvA's 2 GeV neutrino beam energy are quasi-elastic, with just a nucleon and a lepton in the final state. A second third of 2 GeV neutrino interactions are resonant processes in which a  $\Delta$  resonance is created which then decays to a proton + pion, or a neutron + pion. The final third of neutrino interactions at 2 GeV are deep inelastic scattering events where multiple pions are produced. Figure 6.1 illustrates this mix of the neutrino interaction as a function of the neutrino energy, based on a compilation from G. Zeller [1].

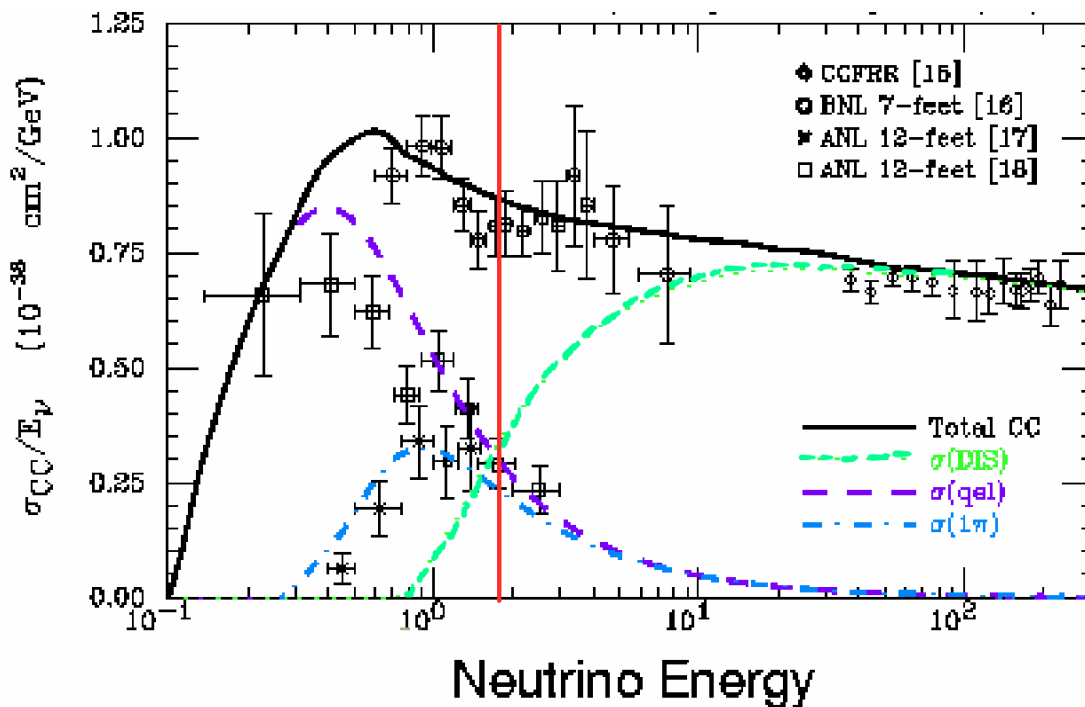


Fig. 6.1: A compilation of low energy charged current neutrino cross sections. The red line indicates the peak energy of NOvA events.

Some selected simulated NOvA events are shown in Figures 6.2 through 6.6 to illustrate properties of the detector. Figure 6.1 shows a simulated quasi-elastic  $\nu_e$  charged current event and Figure 6.2 shows a simulated quasi-elastic  $\nu_\mu$  charged current event. Contrasting these two figures illustrates the NOvA detector's ability to distinguish electrons from muons. Electrons (Figure 6.2) tend to deposit more energy per plane and are more "fuzzy" in the transverse direction to the electron track, having more hits per plane of the detector. Muons (Figure 6.3) tend to leave much longer tracks than electrons, with typically a sharper transverse profile of one hit per plane. Figures 6.2 and 6.3 also illustrate the response of the NOvA detector to protons of energy 1 GeV or less. The protons do not travel far and deposit a large amount of energy in a short distance, typically ending with a large spike of deposited energy as highlighted in the inset of Figure 6.3.

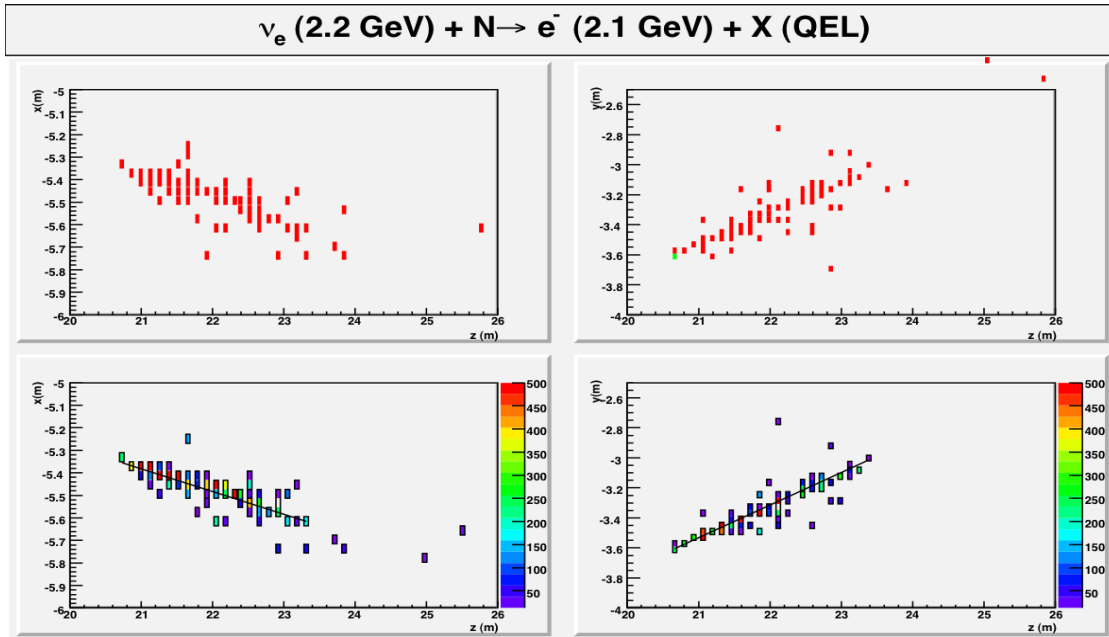


Fig. 6.2: A 2.2 GeV  $\nu_e$  quasi elastic charged current event,  $\nu_e A \rightarrow p e^-$ . The top plots indicate the energy depositions in scintillator in the x-z (*left*) and y-z (*right*) views, color-coded by secondary particle: red for  $e^\pm$  and  $\gamma$ , and a single green deposition from the recoil proton in the y-z view. The bottom plots show event as reconstructed, with pulseheight (ADC,  $\sim 5$  counts/PE) indicated the color scale. The black lines indicate the reconstructed track in the two views.

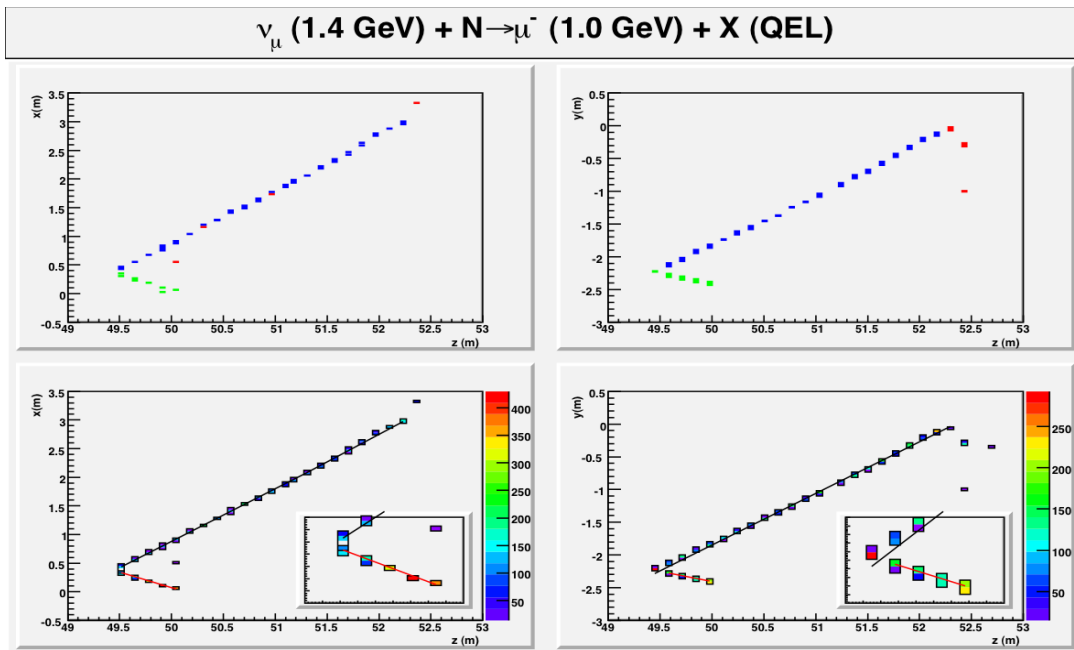


Fig. 6.3: A 1.4 GeV  $\nu_\mu$  quasi elastic charged current event,  $\nu_\mu A \rightarrow p \mu^-$ . The top plots indicate the energy depositions in scintillator in the x-z (*left*) and y-z (*right*) views, color-coded by secondary particle: red for  $e^\pm$  and  $\gamma$ , blue for the muon, and green for the recoil proton. The bottom plots show event as reconstructed, with the color of the boxes indicated pulseheight in photoelectrons. The black and red lines indicate the reconstructed tracks. The inset is a close-up of the vertex, showing the higher pulseheight typical of hits on a proton track.

Figure 6.4 shows a resonant or single pion charged  $\nu_e$  current event in NOvA. The typical pion has a low energy, but can be seen in the detector as a third track. Figure 6.5 shows a deep inelastic scattering  $\nu_e$  charged current event in NOvA with several pions in addition to the outgoing electron. Such multiple pion events are harder to recognize as the 2 GeV of event energy gets divided into more and more parts, but the fuzzy electron can still be identified in many such events.

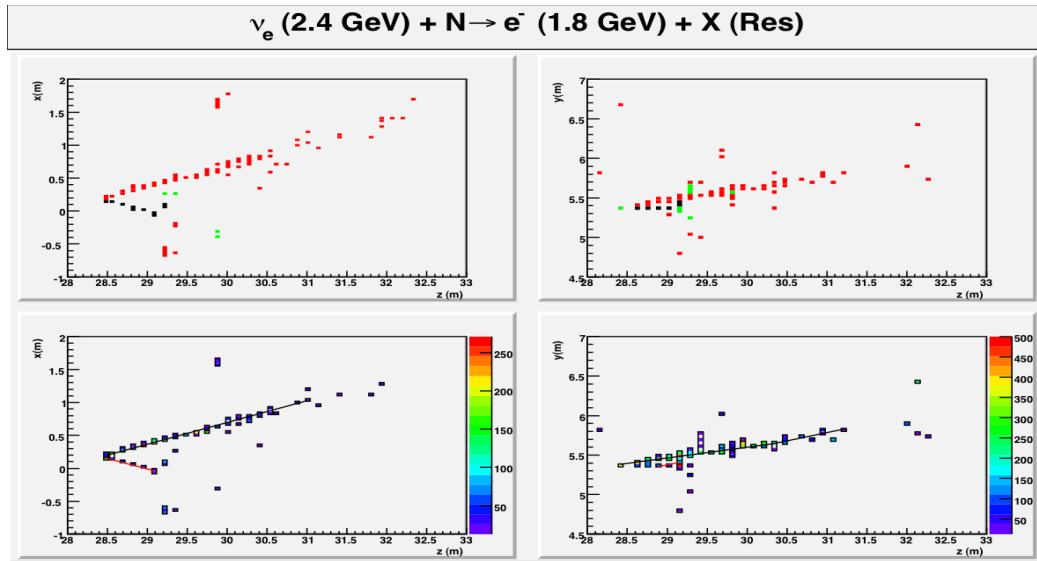


Fig. 6.4: A 2.4 GeV  $\nu_e$  single pion charged current event,  $\nu_e A \rightarrow \Delta^{++} (p \pi^+) e^-$ . The top plots indicate the energy depositions in scintillator in the x-z (*left*) and y-z (*right*) views, color-coded by secondary particle: black for p and  $\pi$  from the  $\Delta^{++}$  decay, red for  $e^\pm$  and  $\gamma$ , blue for the muon, and green for tertiary protons. The bottom plots show event as reconstructed, with the color scale indicating pulseheight. The black and red lines indicate the reconstructed tracks.

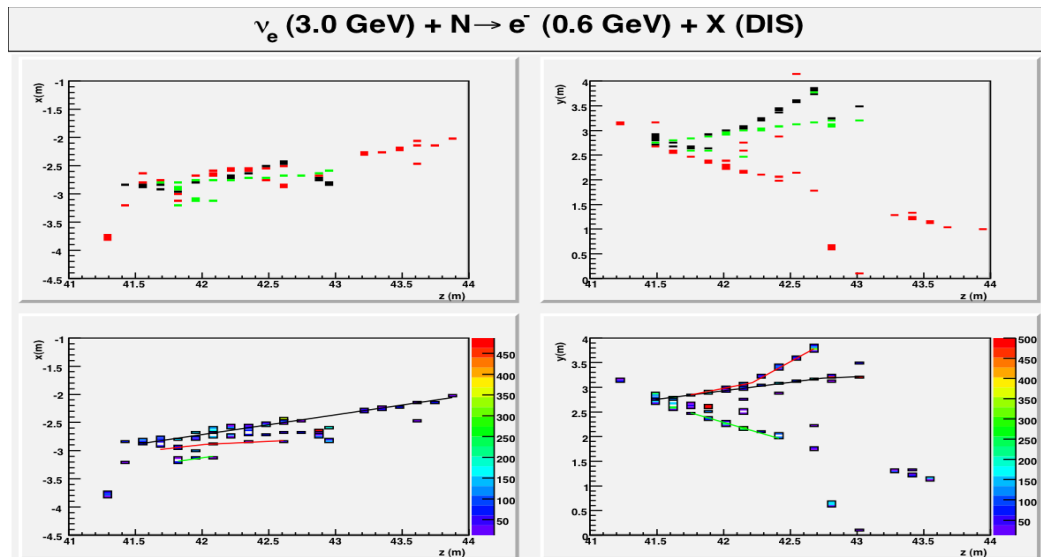


Fig. 6.5: A 3 GeV  $\nu_e$  deep inelastic scattering charged current event,  $\nu_e A \rightarrow p e^- \pi^+ \pi^- \pi^+$ . The top plots indicate the energy depositions in scintillator in the x-z (*left*) and y-z (*right*) views, color-coded by secondary particle: black  $\pi$ , green for protons, red for  $e^\pm$  and  $\gamma$ , blue for the muon. The bottom plots show event as reconstructed, with the color scale indicating pulseheight. The black, green, and red lines indicate the reconstructed tracks.

Neutral current (NC) events with a  $\pi^0$  and the resulting electromagnetic showers in the final state are one of the largest sources of background for the NOvA experiment. Typically, a higher energy neutrino interacts with the nucleus, and the outgoing neutrino takes good fraction of the incoming energy away and is unseen by the detector. The majority of such events are rejected by the identification in at least one view of separate electromagnetic showers from the two photons, and by the gap between the vertex and the first conversion of a  $\pi^0$  decay photon. Figure 6.6 illustrates the exception for a 12.3 GeV NC event, where the reconstruction fails to resolve the two photons due to the overlap of the photons in one view and the short length of one of them in the other view. Furthermore, both photons converted close enough to the event vertex to prevent the resolution of the conversion gap.

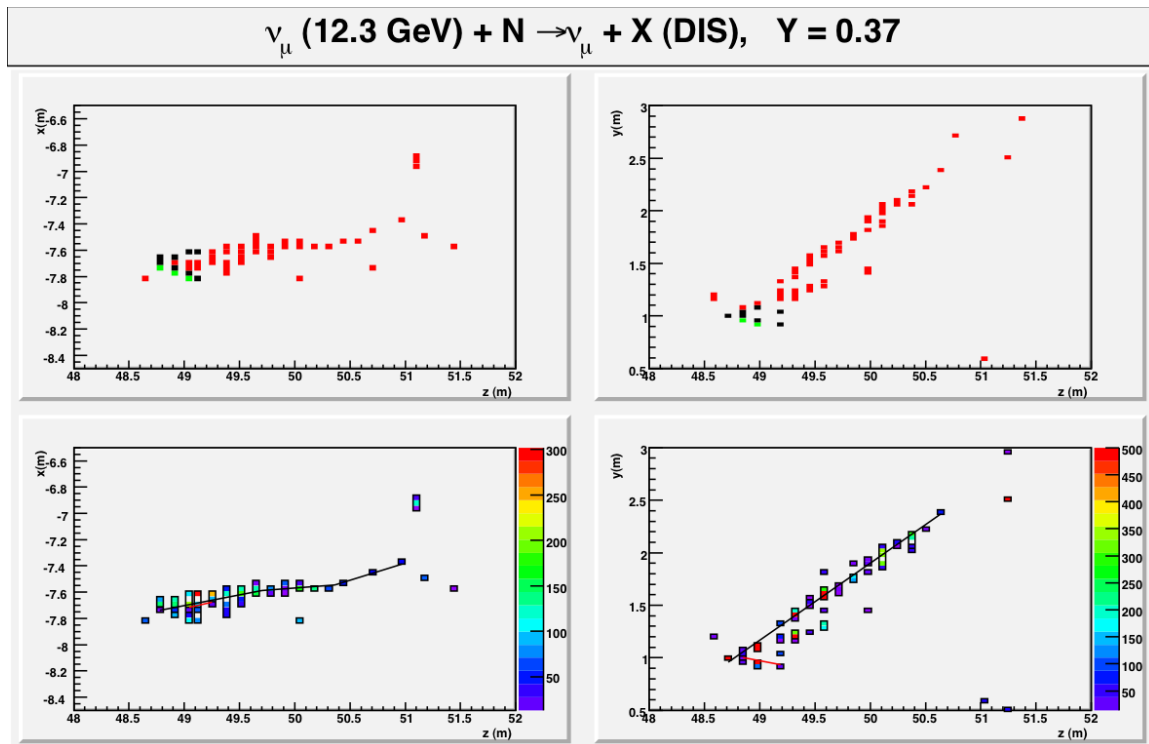


Fig. 6.6: A 12.3 GeV neutral current event,  $\nu_\mu A \rightarrow \nu_\mu p \pi^+ \pi^- \pi^0 (1.21 \text{ GeV}), \pi^0 \rightarrow \gamma \gamma$ . The top plots indicate the energy depositions in scintillator in the x-z (*left*) and y-z (*right*) views, color-coded by secondary particle: black  $\pi$ , green for protons, and red for  $e^\pm$  and  $\gamma$ . The bottom plots show event as reconstructed, with the color scale indicating pulseheight. The black and red lines indicate the reconstructed tracks.

## 6.2 NOvA Performance linked to Cell Light Output and Threshold Cut

### 6.2.1 Technical Requirement on the Threshold Cut.

The NOvA front-end electronics (described in Chapter 14) simply transmits all signals above a preset threshold to the data acquisition (DAQ) system (described in Chapter 15). There are two considerations with regard to the minimum allowable threshold. First, the data rate must be low enough to not overwhelm the DAQ system. Second, the noise must be sufficiently low so as to not affect the pattern recognition of the signal events.

The scale of the data to the DAQ system is set by the cosmic ray rate. We estimate the cosmic ray rate to be approximately 200 Hz with about 200 hits per cosmic ray muon. With 385,000 channels (for 15 kt, 12,036 modules) and 10 bytes per hit, this corresponds to a total hit rate of 40 MHz and a data rate of about 0.5 GB/s. This is discussed in Chapter 15.

A conservative goal would be to limit the noise rate to one-third of the cosmic muon rate, or about 0.17 GB/s. The noise will be dominated by the amplifier noise, but a long tail of noise is seen due to excess noise of the APD amplification, shown in Figure 6.7. Taking the relevant time window to be 1  $\mu$ s, this requirement corresponds to a noise hit probability of  $10^{-4}$ . From Figure 6.1, this gives a minimum threshold of 15 photoelectrons.

The largest events of relevance have a domain of interest approximately 2 m in width and 18 m in length. This corresponds to 15,000 cells, so a random noise probability of  $10^{-4}$  would yield an average of 1.5 noise hits per event. This is clearly an acceptable level.

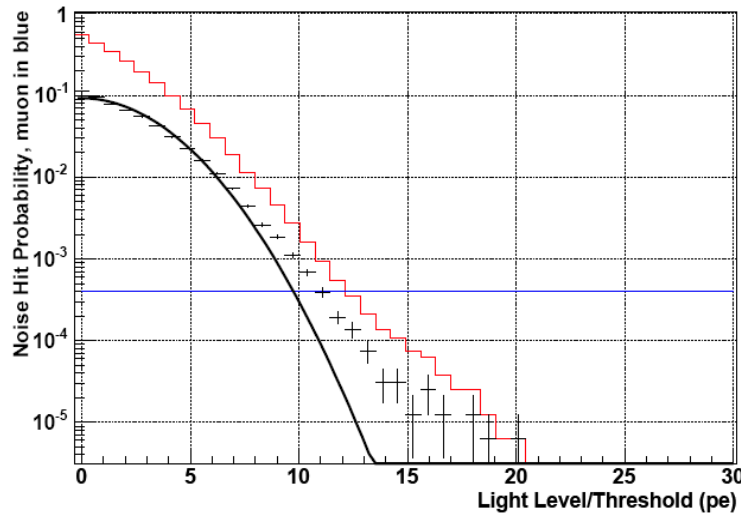


Fig 6.7: Noise hit probability versus the light threshold in photoelectrons. The top (red) histogram gives the integrated hit probability and the (blue) horizontal line is the expected hit probability from cosmic rays. The data points are shown as crosses and the best fit Gaussian, the amplifier noise, is the black line.

Figure 6.7 shows the noise hit probability for the amplifier in our test cell which had a mismatched capacitance to the APD. A new matched ASIC amplifier has been designed and produced, and that amplifier is much quieter with a noise level of  $\sim 150$  electrons compared to the  $\sim 250$  electrons RMS of the amplifier used to produce Figure 6.7. Our expectations for the threshold using the new ASIC amplifier at the same noise hit probability of  $10^{-4}$  are a minimum threshold of 10 photoelectrons.

### 6.2.2 Required Light Level

Given a threshold of 10 - 15 photoelectrons, the next issue is what light level is required to give adequate pattern recognition. Our simulations do not show a strong dependence on the light output as indicated in the Table 6.1 from the NOvA CDR [1]. The table shows that if the mean signal is above the threshold by 25 to 30% there is no loss of sensitivity as measured by the figure of merit (FoM). This would indicate that for our expected noise contributions requiring a threshold of approximately 15 photoelectrons, the required mean light level is 20 photoelectrons. Although we are wary of setting too low a light requirement which could compromise future efforts to improve our analysis algorithms, these simulations indicate that our scientific design criterion on the Figure of Merit (Chapter 4, Table 4.1) translates into a technical requirement for a minimum 20 photoelectrons from the far end of the cell with a photoelectron threshold set at 15.

Signal ( pe )	10	15	20	25
<b>Threshold ( pe )</b>				
10	0.95	1.00	1.02	1.00
15			1.00	
20			0.98	1.00

Table 6.1: Results of simulations showing the relative Figure of Merit for a given threshold and average light output in photoelectrons from a minimum ionizing particle transiting the far end of a NOvA cell.

### 6.3 Measured Performance of Multiple Cells

Our R&D efforts during 2005 - 2007 led to prototype lengths of extrusions with 15% Anatase titanium oxide loaded rigid PVC in a 16-cell wide arrangement. We have used this material to form a 4x3 array of NOvA cells of as shown in Figure 6.11. Several 33.4 meter lengths, 0.7 mm diameter, Kuraray, K27 (Y-11) fluor dye, S-type multiclاد fiber have been inserted into the cells of this array. Fibers with 150, 250, and 200 ppm of K27 dye were used and these fibers were from Kuraray “Batch 1” as described in Chapter 12. The fibers in these test cells have a loop at the far end just like the NOvA design. The complete array of cells shown in Figure 6.11 were immersed in a bath filled with fully oxygenated liquid scintillator equivalent to Bicron BC-517P (see Chapter 10).

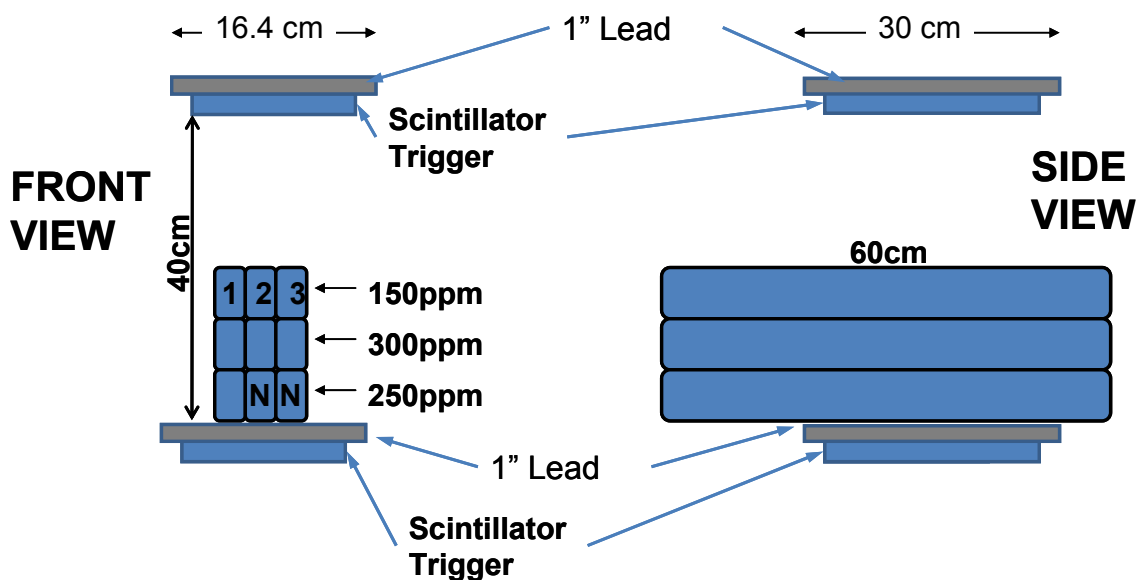


Fig. 6.11: Test cell array used to measure several cells. Ten of the twelve fibers were of Far Detector length and two (“N”) were Near Detector length.

The fiber was connected to a prototype readout using a commercially available Hamamatsu APD array which has pixels of dimensions 1.6mm by 1.6mm. The APD was cooled to -15°C using a TE cooler and was operated at a gain of 100 as in the NOvA design. The APD was readout using the MASDA ASIC chip discussed in section 3.4.6 of the NOvA CDR [2]. This was

an existing version of the chip optimized for 70 picoFarad input capacitance rather than the APD's 10 pF, so the electronic noise in the system was 350 electrons.

A set of scintillator paddles were placed above and below the test cell and pulse heights were recorded from the test cell for cosmic ray muons crossing the 6.0 cm dimension of the test cell. This is the direction most tracks from neutrino events in NOvA will cross the cells. Cosmic tracks at angles to the cell were eliminated by vetoing on any events with observed pulse height in the adjacent cells.

We focus here on the cells with 300 ppm K27 concentration fiber following the optimization discussed in Chapter 12. The distribution of pulse heights observed are shown in Figure 6.12 a), b), and c) for the three 300 ppm cells.

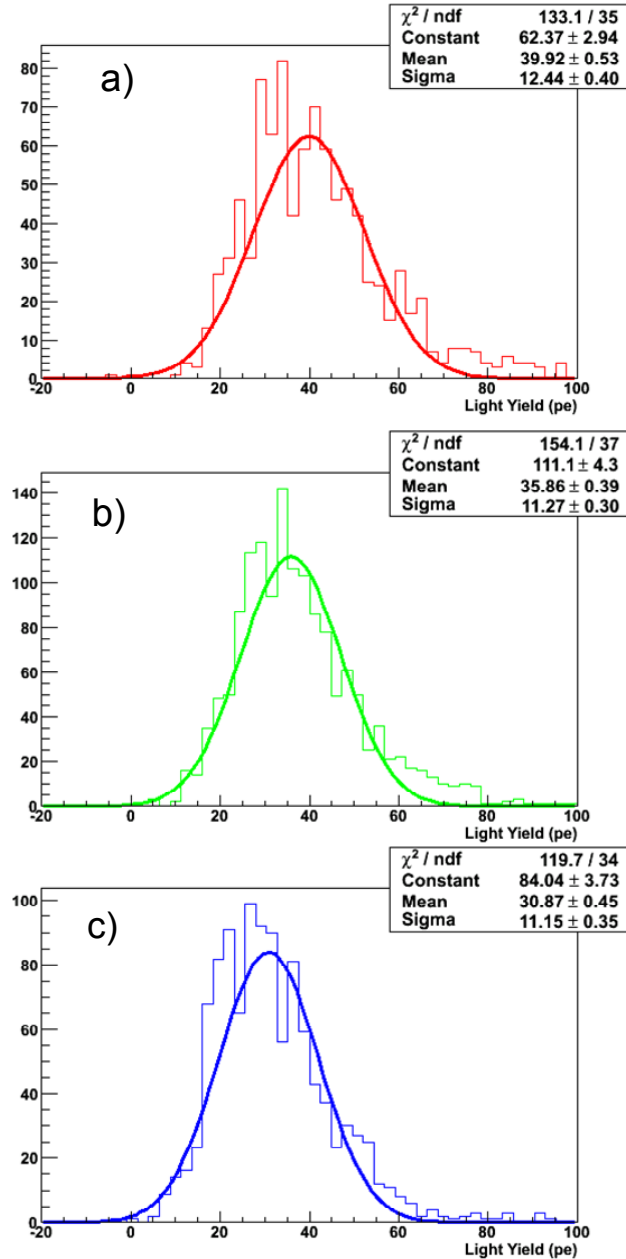


Fig. 6.12: Distribution of pulse heights in photoelectrons from three NOvA cells with 300 ppm K27 0.7mm fiber and Bicorn BC517P scintillator.

Figure 6.12 shows pulse height peaks in the range 31 – 40 photoelectrons. Photostatistics would imply the RMS widths in Figure 6.12 should be given by

$$\text{RMS width} = \text{Sqrt} [(N_{pe} * F) + (e_{RMS})^2],$$

Where  $N_{pe}$  is the Mean of the distribution,  
F is the excess noise factor = 2.5, and  
 $e_{RMS}$  is the electronics RMS noise ( $\sim 4$  for this prototype).

So we expect widths of 10 – 11 photoelectrons and see widths (sigma) of 11 – 12.5 photoelectrons.

The variation in means of the three distributions is presumably due to construction variations and that will be treated in the next section. Our conclusion from Figure 6.12 is that we have demonstrated a mean pulse height of  $\sim 35.5$  photoelectrons from the far end of three standard NOvA cells.

## 6.4 NOvA Scientific Performance Requirement Translated into Design Criteria

Section 6.2 demonstrated that a minimum light level of 20 photoelectrons (p.e.) from the far end of a 15.7 m long NOvA cell is required to meet our scientific design criterion on the Figure of Merit (see Chapter 4). The test cells described in Section 6.3 indicate that our design results in  $\sim 35.5$  p.e. from the far end of a cell, apparently meeting this criterion easily. Ideally all cells in the NOvA detectors would be identical and each would have this same performance. However, the multicell test described in Section 6.2 does not reflect the expected full range of variation since it used only one mixture of scintillator, only one run of PVC extrusions, only one small production run of fiber, and only one prototype APD. In reality we expect wider variations in these component parts that will result in a wider distribution of performance among the 385,000 separate cells.

Recognizing these construction variations, we have elected to set individual technical requirements on each component of the NOvA cell to ensure that all but a handful of cells in an event meet the 20 p.e. requirement. The individual requirements are somewhat arbitrary and are selected to allow for random variations in construction and systematic variations in the procured components. Some of these component requirements are based on cost considerations as we wish to preserve multiple vendors where possible. These criteria will be used as a starting point for additional technical design criteria developed for each component in Chapters 10 through 14.

### 6.4.1 Technical Design Criterion for the NOvA scintillator

We require the NOvA Scintillator to have a light output equivalent to 80% of the light observed at 1 meter in the commercially available scintillator Bicorn BC517P. This criterion includes both light generation and light attenuation in the scintillator during its typical  $\sim 1$  meter path through the scintillator before being absorbed by the fiber. The 80% criterion was arbitrarily chosen to allow a cost reduction in the fluor content of NOvA scintillator. An additional 4% (sigma) is allocated to cover our expected ability to mix the scintillator components to achieve a standard light output. This is discussed further in Chapter 10.

### 6.4.2 Technical Design Criterion for the NOvA Wavelength Shifting Fiber

Relative to the light seen in our tests of 0.7 mm diameter fiber with 300 ppm K27 waveshifter at 16 meters from the light source, we expect the NOvA fiber to have a random distribution with a standard deviation of 16% based on tests described in Chapter 11. Effects

from light absorption by the K27 dye, light attenuation along the fiber, and production variations in the fiber are included here. It is worth noting here that our test cells did not use the highest performance 300 ppm fiber we have obtained (see Chapter 10). The test cell fiber came from Kuraray “batch 1” which measured ~ 7% less light output than Kuraray “batch 2”, but both batches had variations within the batch larger than this difference.

#### **6.4.3 Technical Design Criterion for the NOvA PVC Extrusions**

Nominally the light in the NOvA cell bounces off the PVC wall about 8 times before striking a fiber. Connecting PVC reflectivity to light output via the eighth power of the reflectivity indicates about a  $\pm 1.5\%$  change in light output for the reflectivity variations of about 0.3% observed in our PVC samples (see Chapter 11). We allow a 3% change in light output from the PVC reflectivity.

#### **6.4.4 Technical Design Criterion for the NOvA Extrusion Modules**

As discussed in Chapter 13, we do not control the fiber position inside the NOvA cells in our construction technique. At the looped end, the fiber is constrained to be in opposite corners to control the radius of curvature, but away from the loop the fiber is unconstrained. Simulations [3] indicate that there may be a loss of light if the fiber ends up against a wall or in the corners of the PVC. In studies [4] where the fibers have been forced into these reduced light positions predicted by simulations, we have been unable to measure any effect larger than about 4%. To cover these possible construction effects we assign a 5% random error to the light level due to fiber position in the cell.

#### **6.4.5 Technical Design Criterion for the NOvA Avalanche Photodiodes and Electronics**

We require the APDs to have a random variation of less than  $\pm 5\%$ . This variation includes gain stability, pixel to pixel variations, and effects from alignment variations of the fibers to the pixels. This is discussed further in Chapter 14.

#### **6.4.6 Aging Effects**

We allow a 10% random degradation due to unknown aging effects in the NOvA cells. We do not expect any particular aging effects based on earlier detectors [5]ref CDR chapters where we discussed this], but are still engaged in accelerated and real time aging tests to see if any component acts on another over time.

#### **6.4.7 Summary of Technical Design Criteria**

Using the minimum requirements set in the previous six sections, our measured 35.5 photoelectron light level with BC-517P can be reduced by the one scintillator systematic effect to

$$(35.5 \text{ photoelectrons}) \cdot (0.8 \text{ for the scintillator minimum}) = 28.4 \text{ photoelectrons}$$

The random effects in the previous six sections are added in quadrature, resulting in an additional variation of

$$\sqrt{(0.04)^2 + (0.16)^2 + (0.03)^2 + (0.05)^2 + (0.05)^2 + (0.10)^2} = 20.6\% \text{ (sigma)}$$

Our observed fluctuations in mean pulse height among the three test cells discussed in section 6.3 are consistent with this 20.6% sigma estimate.

The random effects variation of 20.6% implies the 1 sigma change in light on a 28.4 p.e. light level would be about 5.9 p.e., which is 1.4 sigma away from our desired minimum of 20 p.e. Assuming a Gaussian distribution, the area on the low side tail  $> 1.4$  sigma below 20 p.e. would be about 8 % of the cells. Given a typical event track length of  $\sim 120$  cells for a 2 GeV  $\nu_\mu$  CC event, this would mean about 5 of the 60 vertical cells in such an event would fail the 20 photoelectron requirement if the event occurred at the far bottom edge of the detector. Similarly 5 of the 60 horizontal cells would fail the 20 photoelectron requirement if the event occurred at the far east edge of the detector. This is acceptable, but we conclude that a mean light level of 28.4 photoelectrons from the far end of a NOvA cell is not excessive and instead insures the experiment against expected fluctuations in construction.

## 6.5 Quantitative Performance Analysis of the NOvA Far Detector

### 6.5.1 Simulation and Reconstruction Package

The NOvA Far Detector performance in the identification of signal and background for the  $\nu_\mu \rightarrow \nu_e$  measurement has been studied using a detailed Monte Carlo simulation and reconstruction package. The simulation is a version of the highly developed GEANT-based package used by the MINOS collaboration, with appropriate changes to the detector geometry, composition, readout, and location. The reconstruction algorithm applies a Hough transform to the simulated digitizations to find track-like objects in each view. The objects are combined in the two views, and used to form a reconstructed event.

Neutrino oscillations are considered with the parameters of  $\sin^2(2\theta_{13}) = 0.10$ ,  $\sin^2(2\theta_{23}) = 1.0$ , and  $\Delta m_{32}^2 = 0.0024 \text{ eV}^2$ , without matter effects and without interference between solar and atmospheric scale transitions. The numbers of events described in this section are normalized to the expectation for a 15 kT detector with  $18 \times 10^{20}$  protons on target each for neutrino and anti-neutrino running.

Background events to the  $\nu_e$  appearance charged current (CC) signal are divided into three classes:  $\nu_\mu$  CC, neutral current (NC), and intrinsic beam  $\nu_e$ . Electron neutrino CC signal events have electrons that generate electromagnetic showers, while muons from  $\nu_\mu$  CC have clear straight track and are easily distinguished with the performance of NOvA Far Detector. Most of NC background events have more diffused patterns of hits at lower typically pulseheights, but occasionally have multiple electromagnetic showers induced from decay of  $\pi^0$ , and thus are a potential background to the  $\nu_e$  CC signal. The intrinsic beam  $\nu_e$  CC differ from the  $\nu_e$  CC appearance signal only in energy spectrum, so despite their small overall contribution to the beam, they also contribute substantially to the total background.

Following a pre-selection based on total event length, total pulseheight, and the number of planes in the primary track, an Artificial Neural Network (ANN) technique is employed to discriminate  $\nu_e$  CC appearance signal events from background. The ANN is trained with 19 variables characterizing reconstructed events. Generalizing from the specific examples in the preceding section, for example, the range of the primary reconstructed track shown in Figure 6.13 (a) tends to be longer for  $\nu_\mu$  CC and shorter for NC backgrounds than typical  $\nu_e$  CC signals. Figure 6.13 (b) shows the distribution of charge/range (equivalent to  $dE/dx$ ) of reconstructed tracks. The distribution for muon tracks in  $\nu_\mu$  CC background events is sharply peaked compared to that of the signal. The other variables utilize the number of reconstructed tracks, fraction of hits in the primary track, track profile of the primary and sub-tracks, etc. Figure 6.14 shows the discrimination of  $\nu_e$  CC signal from the backgrounds in the ANN output parameter.

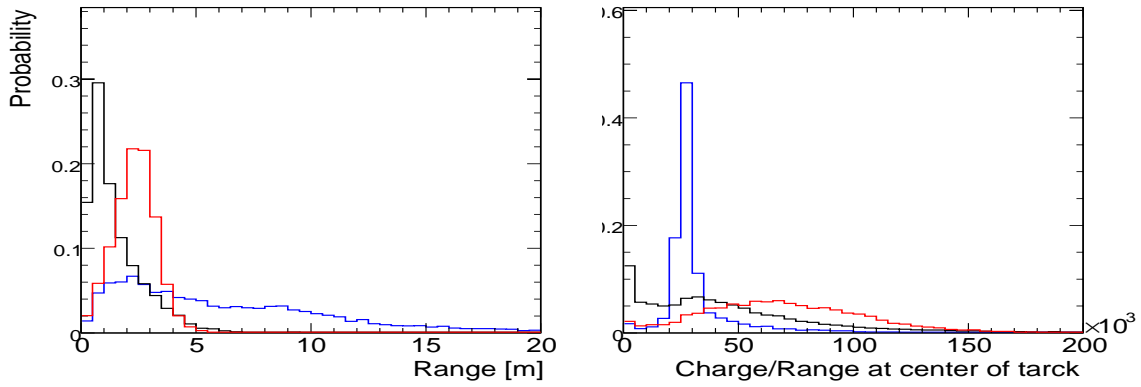


Fig. 6.13: Range (a) and charge/range (b) of reconstructed track in the NOvA Far Detector oriented parallel to the neutrino line of flight. The red histograms show the probability distribution for  $\nu_e$  CC signal; blue and black histograms show  $\nu_\mu$  CC and NC background.

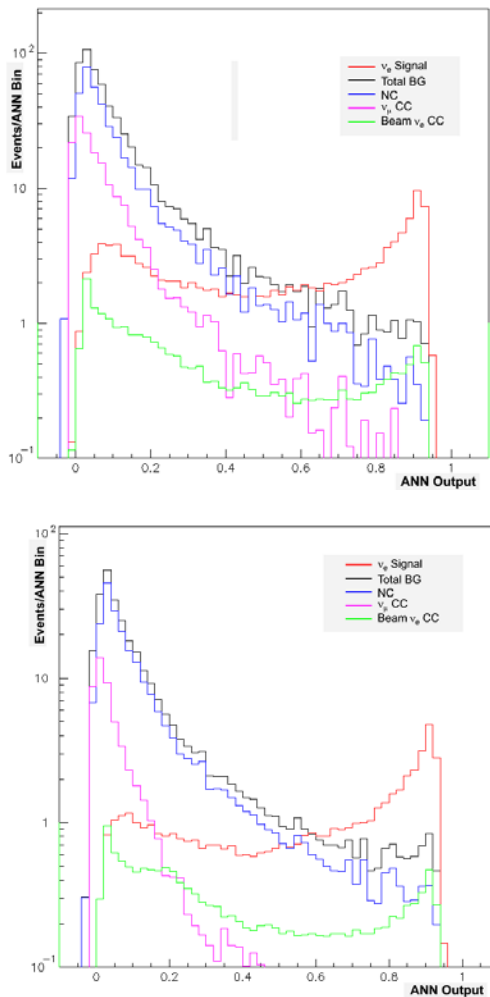


Fig. 6.14: Output parameter of ANN for  $\nu_e$  CC for neutrino running (*top*) and anti-neutrino running (*bottom*). The numbers of events are normalized to the expectations from  $18 \times 10^{20}$  protons on NuMI target with 15 kton NOvA Far Detector, assuming the oscillation parameters described in the text.

### 6.5.2 Figure of Merit

The Figure of Merit (FoM, see Chapter 4), defined as the number of signal events divided by the square root of the background, is calculated to evaluate the relative sensitivity of the reconstruction and selection algorithms. In the high statistics limit, a higher FoM corresponds to better sensitivity to  $\sin^2(2\theta_{13})$ . Figure 6.15 (6.16) shows the FoM as a function of the number of accepted signal events for neutrino (anti-neutrino) running.

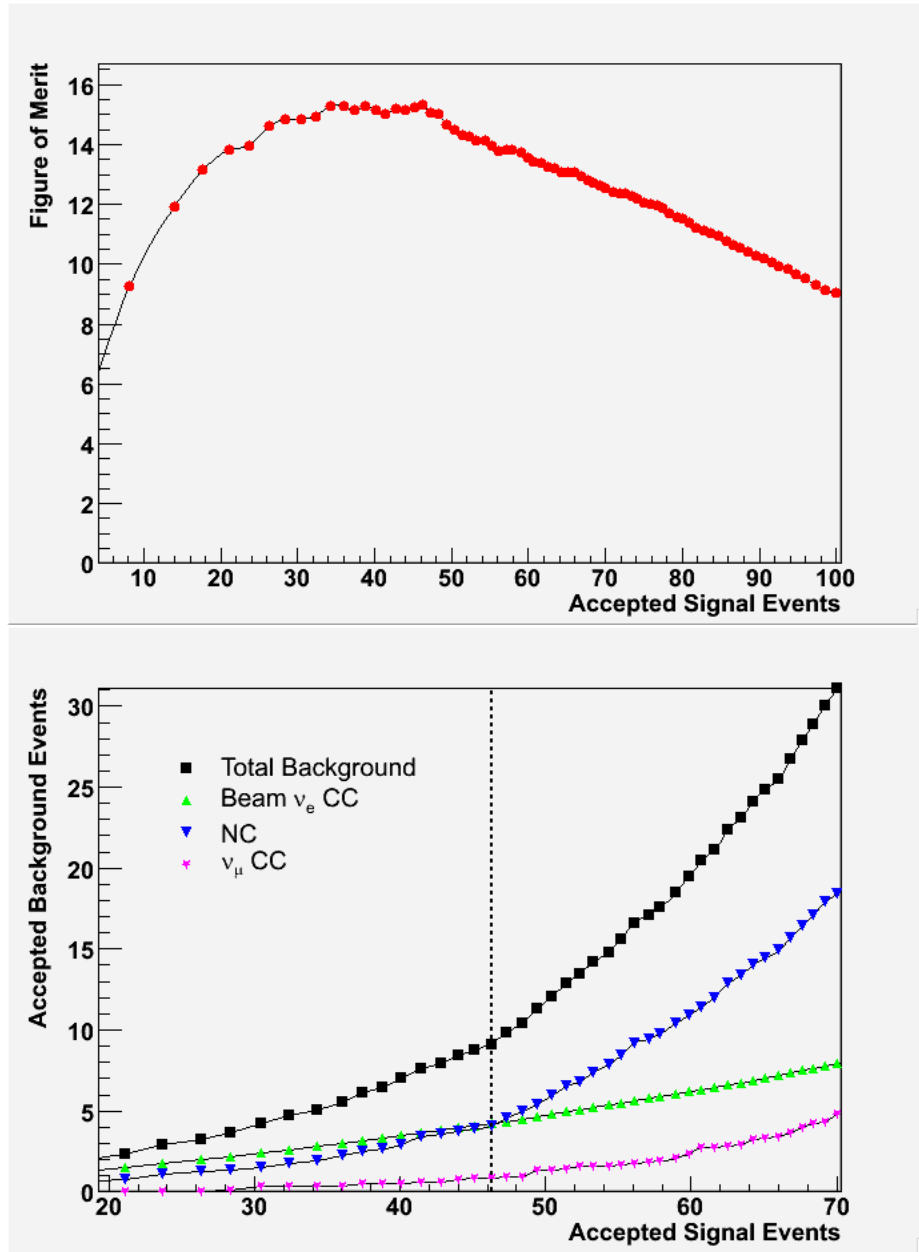


Fig. 6.15: The FoM (*top*) and the numbers of background events (*bottom*) vs. the number of accepted signal events passing the ANN selection parameter cut, in a  $18 \times 10^{20}$  POT neutrino-mode run with a 15kT detector and assuming the oscillation parameters given in the text. The dashed line in the bottom plot indicates the selection corresponding to the highest FOM. Note the different horizontal scales on the two plots.

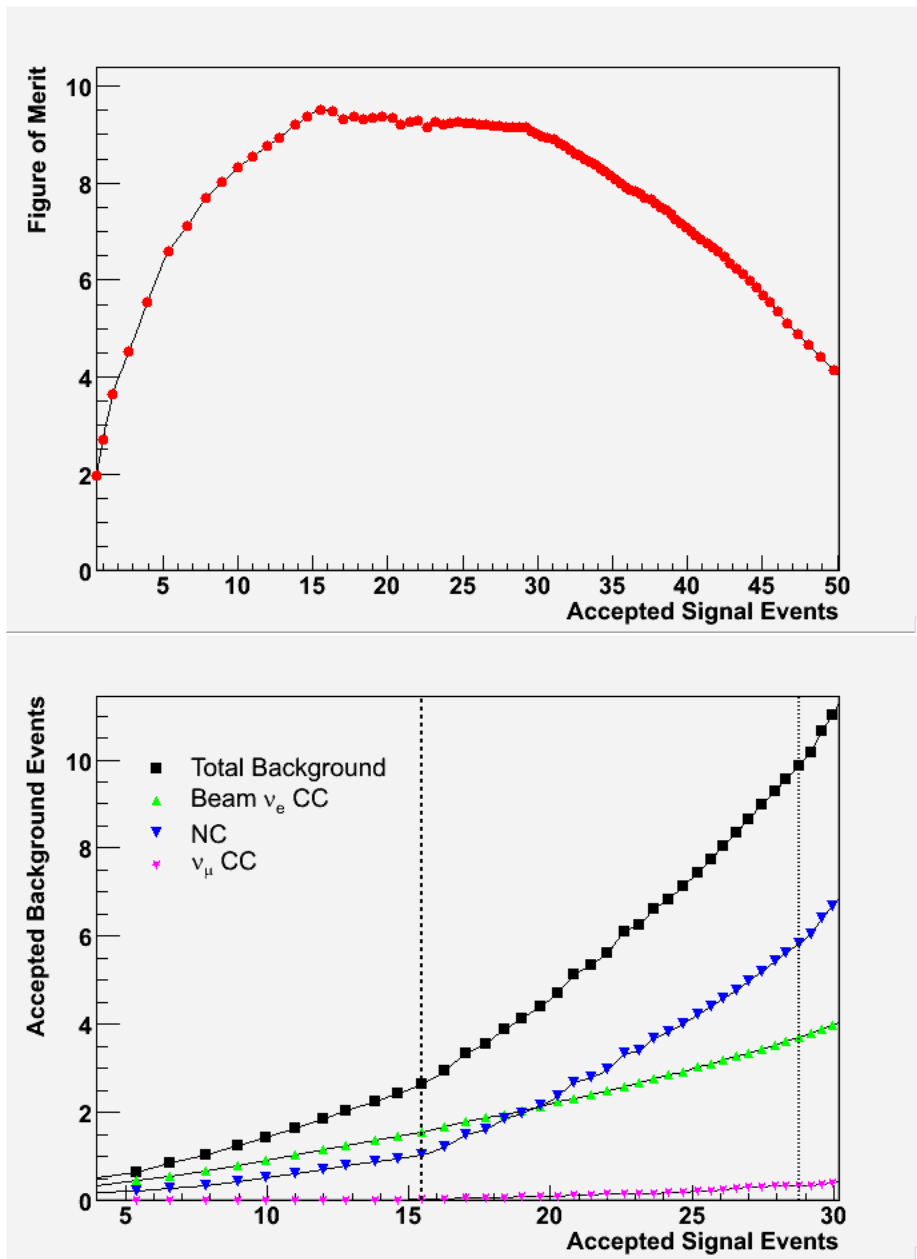


Fig. 6.16: The FoM (*top*) and the numbers of background events (*bottom*) vs. the number of accepted signal events passing the ANN selection parameter cut in  $18 \times 10^{20}$  POT anti-neutrino run with a 15kT detector and assuming the oscillation parameters given in the text. The dashed line in the bottom plot indicates the selection corresponding to the highest FOM; the dotted line indicates a selection with lower FOM but higher efficiency, resulting in optimal  $\sin^2(2\theta_{13})$  reach. Note the different horizontal scales in the two plots.

The obtained FoM is effectively flat between 15 % and 25% (20% and 40%) signal efficiency for neutrino (anti-neutrino) running, and is almost independent on the cut value of ANN parameter in these ranges. The bottom half of Figures 6.15 and 6.16 show the number of each class of background events as a function of the accepted events. The maximum FoM obtained is 15.3 at an ANN cut value of 0.74 for neutrino running, and 9.5 at an ANN cut of 0.8 for anti-neutrino running, yielding a combined FoM of 18.0. However, due to the lower statistics of anti-neutrino running, the optimal sensitivity is achieved with higher efficiency and a reduced FoM of 9.2, corresponding to an ANN cut of 0.56. These selections yield 46.3 (28.8)  $\nu_e$  and  $\nu_e$ -bar CC appearance signal events. The total number of background events with the same criteria is 9.1 (9.8), as shown in Table 6.2. The number of signal events is proportional to  $\sin^2(2\theta_{13})$ , while the number of background events is essentially independent of  $\sin^2(2\theta_{13})$ . The overall efficiency for  $\nu_e$  CC signal events from  $\nu_\mu \rightarrow \nu_e$  oscillations is 26% (41%). The accepted fractions of signal and background are summarized in Tables 6.3 and 6.4.

	FoM	ANN Cut	$\nu_e$ signal	Total BG	$\nu_\mu$ CC	NC	$\nu_e$ beam
Neutrino	15.3	0.74	46.3	9.1	0.8	4.1	4.2
Anti-Neutrino	9.5	0.80	15.5	2.7	0.05	1.0	1.6
Anti-Neutrino	9.2	0.56	28.8	9.8	0.3	5.8	3.7

Table 6.2: Event selection statistics for the selections maximizing the FoM for neutrino running, and the high-efficiency selection for anti-neutrino running.

	$\nu_e$ signal	$\nu_\mu$ CC	NC	$\nu_e$ beam	Total BG
Reconstruction and Fiducial Cut	87.0%	78.1%	55.1%	89.3%	62.1%
Pre-selection	70.6%	18.9%	17.7%	44.0%	18.5%
ANN cut	29.9%	0.1%	0.3%	8.3%	0.4%
Total eff.	26.0%	0.1%	0.2%	7.4%	0.3%

Table 6.3: Efficiency of  $\nu_e$  CC signal and background events for the optimal ANN cut of 0.74, for neutrino running. The efficiency of the ANN cut is relative to the number of events passing the preselection. The total efficiencies are cumulative.

	$\nu_e$ signal	$\nu_\mu$ CC	NC	$\nu_e$ beam	Total BG
Reconstruction and Fiducial Cut	87.4%	76.7%	51.6%	89.8%	58.9%
Pre-selection	73.7%	0.3%	16.3%	70.9%	13.1%
ANN cut	46.8%	0.1%	0.8%	11.6%	0.9%
Total eff.	40.9%	0.1%	0.4%	10.5%	0.5%

Table 6.4: Efficiency of  $\nu_e$  CC signal and background events for the optimal ANN cut of 0.56, for anti-neutrino running. The efficiency of the ANN cut is relative to the number of events passing the preselection. The total efficiencies are cumulative.

### 6.5.3 Detector Energy Resolution for Neutrino Events

The energy resolutions of the NOvA detector for electrons and muons are shown in Figures 6.17 and 6.18.

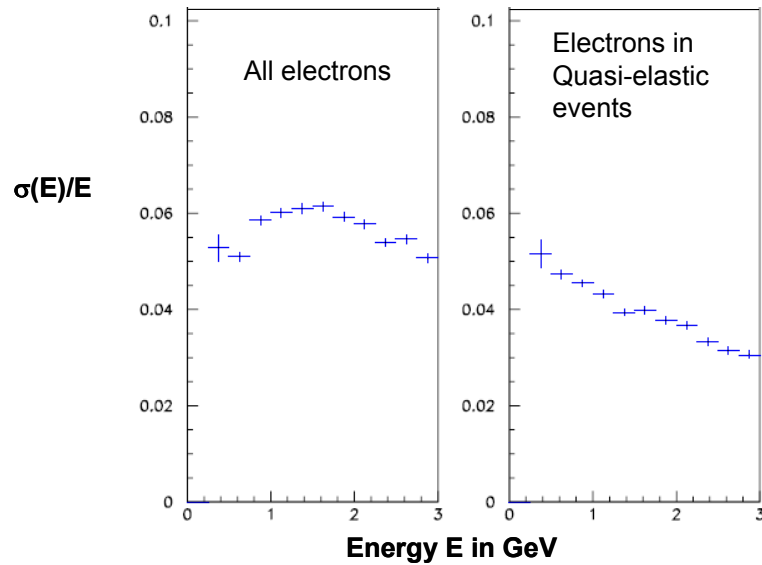


Fig. 6.17:  $\sigma(E)/E$  for electrons in NOvA. The left plot is for all  $\nu_e$  events, while the right plot is for quasi-elastic events only.

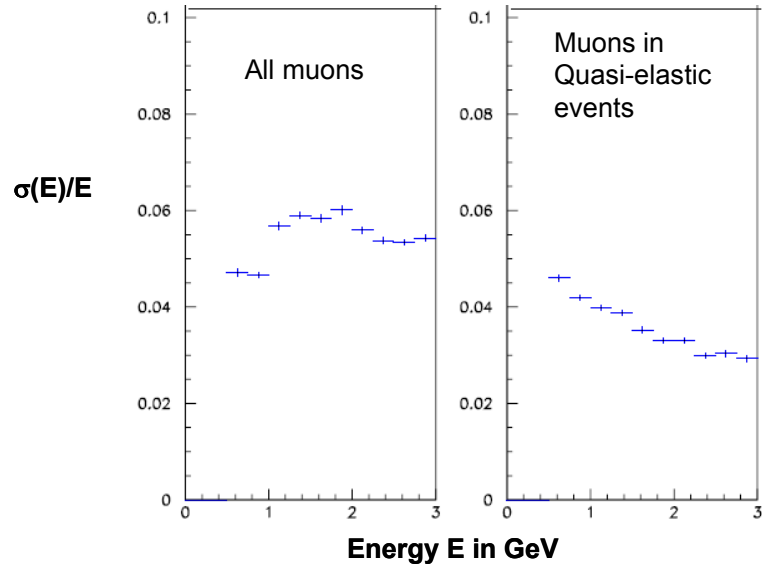


Fig. 6.18:  $\sigma(E)/E$  for muons in NOvA. The left plot is for all  $\nu_\mu$  events, while the right plot is for quasi-elastic events only.

The differences between all events and the quasi-elastic events reflect the mix of events as a function of energy shown in Figure 6.1. At about 0.5 GeV, the quasi-elastic events constitute 75% of all events so the left and right sides of Figures 6.17 and 6.18 agree at that energy. At 2 GeV, where most of the NOvA  $\nu_e$  signal appears, the energy resolution  $\sigma(E)/E$  is about 6% for electrons. For 2 GeV muons, the energy resolution  $\sigma(E)/E$  is about 3.5% for quasi-elastic events.

## 6.6 Simulated Performance of the NOvA Near Detector

### 6.6.1 Location and Orientation

The NOvA Near Detector will be used to characterize backgrounds to the  $\nu_e$  oscillation signal due to misidentified  $\nu_\mu$  CC and NC events, and the intrinsic beam  $\nu_e$  content. It will also be used to characterize the unoscillated  $\nu_\mu$  flux for the high precision disappearance measurement. As shown below, the event rate in each 1 GeV energy bin in the near detector will correspond to statistical errors of 1% or better within  $4 \times 10^{20}$  protons on the NuMI target.

The Near detector will be situated approximately 200 feet downstream of the entry shaft to the MINOS access shaft as shown in Figures 5.8 and 5.9. The mean hadron decay position for  $\nu_\mu$  that interact in the fiducial volume of the near detector at this location is approximately 184 m from the target. The detector will be positioned transversely to the beam axis to maximize the similarity between the Near and Far detector spectra. It will also be oriented at an angle of 14.6 mrad with respect to the NuMI central beam axis direction in the horizontal plane to have a mean neutrino line of flight parallel to the detector horizontal axis, as in the Far Detector.

### 6.6.2 Comparison of Event Spectra between Near and Far Detectors.

The fiducial volume in the Near detector is defined accepting neutrinos interacting at least 40 cm away from the edges of the detector in the x (horizontal) and y (vertical) transverse directions. Along the detector axis, interactions are accepted in the range  $0.53 \text{ m} < z < 3.70 \text{ m}$  for  $\nu_\mu$  charged current (CC) and neutral current (NC) events (9.2 tons), and  $0.53 \text{ m} < z < 8.5 \text{ m}$  for  $\nu_e$  CC events (21 tons).

The Monte Carlo truth neutrino energy spectrum for  $\nu_\mu$  CC events is shown in Figure 6.19 for the Near and Far detectors, normalized to a Near detector exposure of  $4 \times 10^{20}$  protons. The large difference in the shape of spectra between the two is due to the established  $\theta_{23}$  oscillation effect.

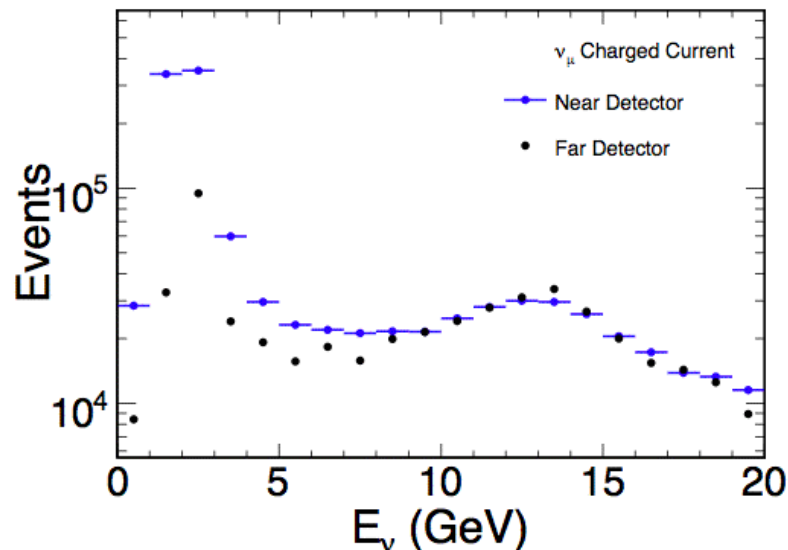


Fig. 6.19: The Monte Carlo (truth) neutrino energy spectrum in  $\nu_\mu$  CC events, for the Near and Far Detectors.

Figure 6.20 compares the  $\nu_\mu$  NC spectra in the two detectors. Since flavor oscillations are not manifest in the NC case, the differences in the two arise solely from the large variation among neutrino parent decay positions relative to the distance to the Near detector, compared to the effective point source of neutrinos for the Far detector. That is, the Near Detector sees a line source of neutrinos while the Far Detector sees a point source. However, since the mean decay angle for neutrinos traversing both detectors is the same, the spectra are very similar. This similarity will make the prediction of neutral current backgrounds in the Far detector based on observations in the Near less dependent on detailed modeling of the parent hadron beam and neutrino interactions. The Monte Carlo intrinsic beam  $\nu_e$  CC spectra for the two detectors are shown in Figure 6.21.

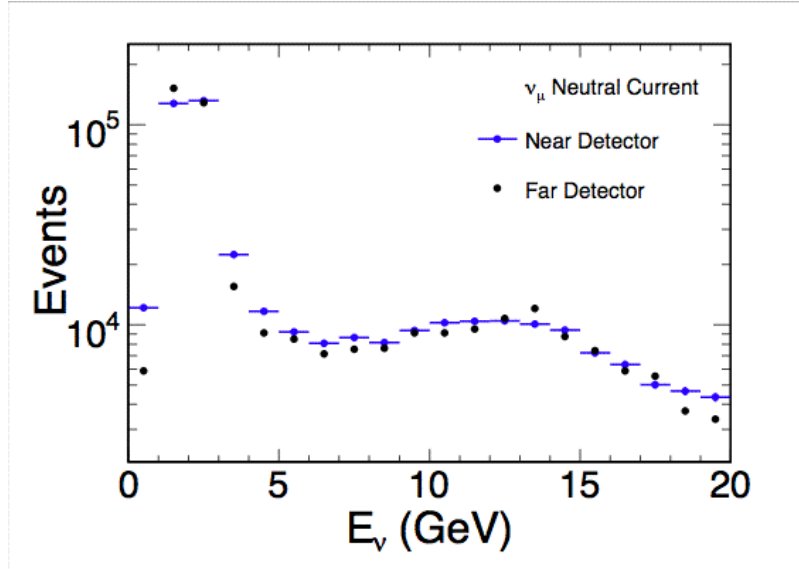


Figure 6.20: The Monte Carlo (truth) neutrino energy spectrum in  $\nu_\mu$  NC events in the Near and Far detectors.

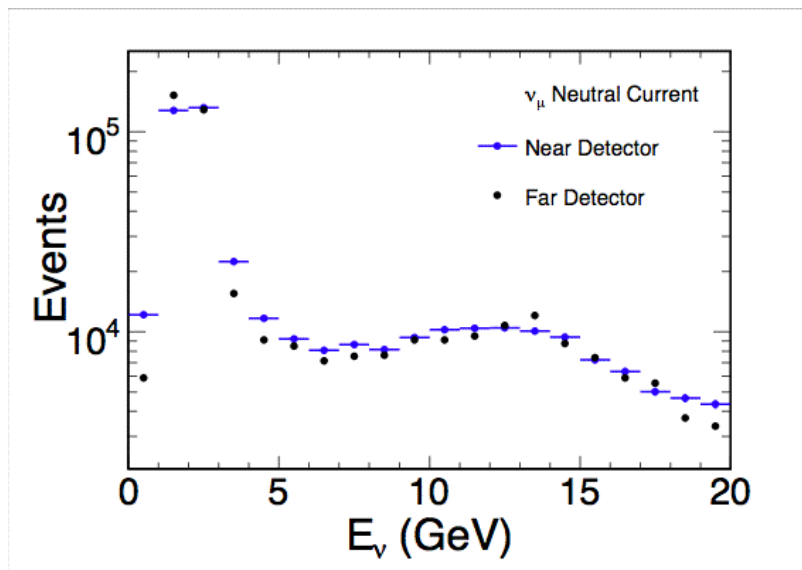


Figure 6.21: The Monte Carlo (truth) neutrino energy spectrum in  $\nu_e$  CC events in the Near and Far detectors. The Far detector spectrum shown is without any  $\nu_e$  appearance oscillation effect.

### **6.6.3 *Near Detector Timing Requirements***

Due to the proximity to the neutrino source, the Near Detector sits in a high event rate environment. In addition to neutrino interactions occurring in the detector, interactions occurring in the rock upstream and to the side of the detector contribute activity in the form of muons, neutrons, and other particles.

Preliminary Monte Carlo studies of the full rate of rock and detector interactions have been conducted for the Near detector in downstream cavern. In an average spill of  $4 \times 10^{13}$  protons on the NuMI target, about 25 interactions occurring in the rock and about 2 contained neutrino interactions contribute to the visible activity in the Near Detector. Given the topology of both classes of events, it is expected that events separated spatially by more than 2.5 m will usually be reconstructed correctly. At smaller distance separations, such as occurs in the single simulated spill of  $4 \times 10^{13}$  protons on target shown in Fig. 6.22, timing information from the front-end electronics will often be needed to correctly reconstruct the two events, as is the case in the spill shown.

Figures 6.23 and 6.24 show two time slices of activity in the same spill, assuming  $1.5 \mu\text{s}$  double pulse separation. In this case, such separation is sufficient to correctly identify the two detector interactions contained in the spill, which occurred  $1.76 \mu\text{s}$  apart. In general, however, the potential for improvements in proton intensity and other contingencies will make a finer timing separation desirable.

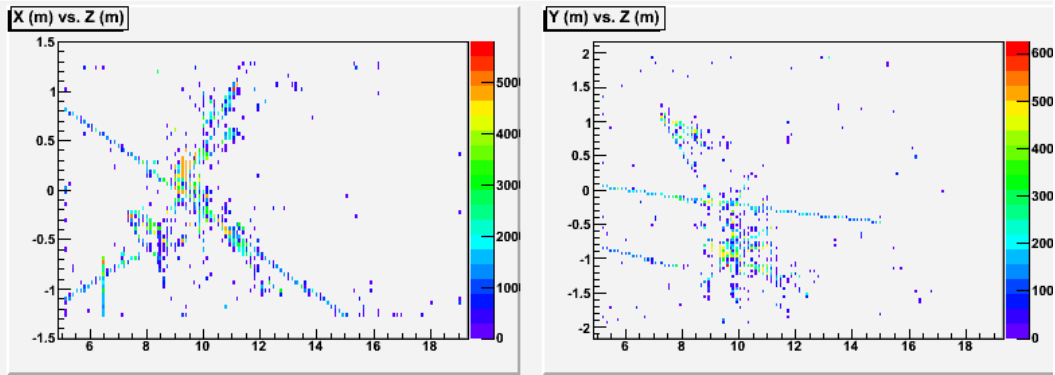


Figure 6.22: The ensemble of simulated digitizations in the X-Z and Y-Z views, from a single beam spill of  $4 \times 10^{13}$  protons on target. In these views, the front (upstream) end of the detector is at  $Z=5$  m.

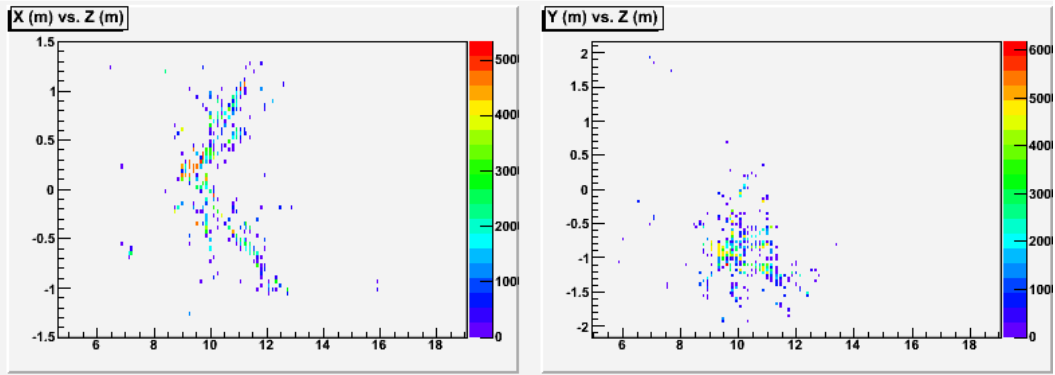


Figure 6.23: A  $1.5 \mu\text{s}$  time slice from the spill shown in Fig. 6.20. Most of the remaining activity is from a single interaction in the detector:  $\nu_\mu (11.8 \text{ GeV}) + \text{N} \rightarrow \mu + \text{X}$  ( $y=0.98$ ).

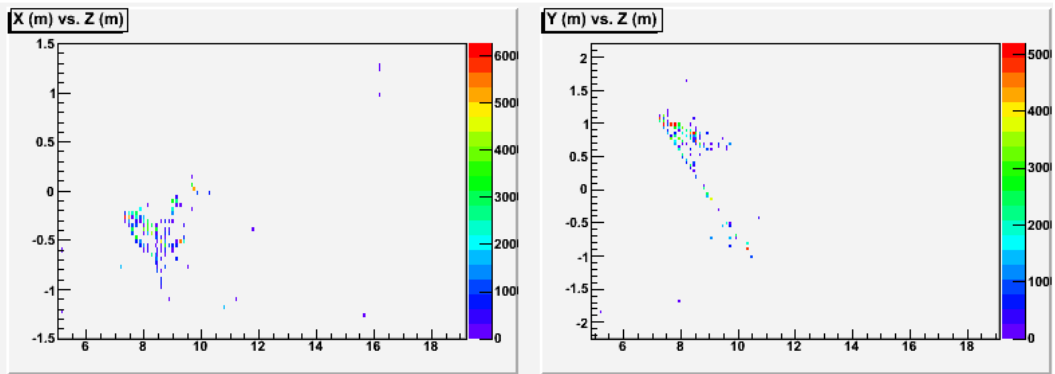


Figure 6.24: Another  $1.5 \mu\text{s}$  time slice from the spill shown in Fig. 6.20. Most of the remaining activity is from a single interaction in the detector:  $\nu_\mu (8.9 \text{ GeV}) + \text{N} \rightarrow \nu_\mu + 3\pi^0$  ( $y=0.29$ ).

## 6.7 Summary: NOvA Design Performance vs. Scientific Design Criteria

Table 6.3 compares the simulated performance of the selected NOvA design to the scientific design criteria discussed in Chapter 4. All the design criteria are met.

Design Parameter	Scientific Design Criterion	Performance of the NOvA Preliminary Design
Distance off-axis	11.5 to 12.0 km	11.77 km
Distance from Fermilab	As far from Fermilab as practically possible.	810 km, farthest possible site in the United States along the NuMI beamline
Experimental Sensitivity	Figure of merit greater than or equal to 18  <i>The Figure of Merit is defined as the number of <math>\nu_e</math> signal events divided by the square root of the background for <math>36 \times 10^{20}</math> protons on the NuMI target equally divided between neutrino and anti-neutrino focusing at the oscillation values <math>\sin^2(2\theta_{13}) = 0.1</math> and <math>\Delta m^2_{32} = 0.0024 \text{ eV}^2</math> without regard to matter and atmospheric-solar interference effects.</i>	FoM = 18
Energy resolution for $\nu_e$ Charged Current events	Less than 8% at 2 GeV	6% at 2 GeV
Energy resolution for Quasi-Elastic $\nu_\mu$ Charged Current events	Less than 4% at 2 GeV	3.5% at 2 GeV
Far Detector overburden	> 10 radiation lengths	4 feet of concrete plus 0.5 feet of barite = about 14 radiation lengths
Near Detector	a) At least a 20 ton fiducial volume located about 1 kilometer from the NuMI target with sufficient transverse and longitudinal size for neutrino event containment.  b) Segmentation in the fiducial volume identical to the Far Detector.  c) Orientation identical to the Far Detector	a) 21 ton fiducial volume, located at 1.02 km from the NuMI target The transverse fiducial volume is 40 cm from all edges, and the longitudinal fiducial volume is followed by a 4.75 m containment region.  b) identical construction in the fiducial volume  c) Identical orientation.

Table 6.3: NOvA Design Parameters. The scientific Design Criteria and the performance of the preliminary NOvA design are given for each parameter.

## 6.8 Chapter 6 References

- [1] G. Zeller, “Low-energy neutrino cross sections: comparison of various Monte Carlo predictions to experimental data”, hep-ex/0312061, Proceedings of NuInt’02, Irvine CA, December 2002.
- [2] NOvA Conceptual Design Report, Chapter 5, Section 5.3, March 31, 2006, NOVA-doc-536. The CDR is also available at <http://www-nova.fnal.gov/>.
- [3] C. Howcroft, February 2007, NOVA=doc-1418. See also CDR [2], Chapter 12, Section 3.
- [4] D. Cronin-Hennessy, August 2005, NOVA-doc-139.
- [5] For examples, see the CDR [2], Chapter 10, Section 6.